Cells and Materials

Volume 3 | Number 1 Article 8

1993

Metallurgical Structures of As-Cast and Heat-Treated High-Palladium Dental Alloys

William A. Brantley
The Ohio State University

Zhuo Cai
The Ohio State University

Alan B. Carr
The Ohio State University

John C. Mitchell
The Ohio State University

Follow this and additional works at: https://digitalcommons.usu.edu/cellsandmaterials

 Part of the Biomedical Engineering and Bioengineering Commons

Recommended Citation

Brantley, William A.; Cai, Zhuo; Carr, Alan B.; and Mitchell, John C. (1993) "Metallurgical Structures of As-Cast and Heat-Treated High-Palladium Dental Alloys," *Cells and Materials*: Vol. 3 : No. 1 , Article 8.
Available at: https://digitalcommons.usu.edu/cellsandmaterials/vol3/iss1/8

This Article is brought to you for free and open access by the Western Dairy Center at DigitalCommons@USU. It has been accepted for inclusion in Cells and Materials by an authorized administrator of DigitalCommons@USU. For more information, please contact digitalcommons@usu.edu.

Cells and Materials, Vol. 3, No. 1, 1993 (Pages 103-114)
Scanning Microscopy International, Chicago (AMF O'Hare), IL 60666 USA

1051-6794/93$5.00+.00

METALLURGICAL STRUCTURES OF AS-CAST AND HEAT-TREATED HIGH-PALLADIUM DENTAL ALLOYS

William A. Brantley[1,*], Zhuo Cai[1], Alan B. Carr[1], and John C. Mitchell[2]

[1]College of Dentistry and [2]Department of Geological Sciences
The Ohio State University, Columbus, Ohio 43210

(Received for publication December 28, 1992, and in revised form March 9, 1993)

Abstract

Scanning electron microscope observations and energy-dispersive spectroscopic analyses have been performed on two first-generation and two second-generation high-palladium dental casting alloys. A specimen design simulating a maxillary central incisor coping was employed to conserve metal, while providing thin and thick sections to yield a range of solidification rates. The alloys were centrifugally cast in air, following standard dental laboratory techniques; three castings were prepared for each alloy. Each casting was sectioned to produce two mirror-image specimens, and one specimen received the appropriate oxidation heat treatment, followed by a simulated full porcelain firing sequence. After metallographic polishing, specimens were examined with a scanning electron microscope. The as-cast alloys displayed multi-phase microstructures which could be explained by the rapid solidification conditions and the relevant phase diagrams. The simulated porcelain firing heat treatment caused a variety of bulk microstructural changes in the coping sections, along with formation of complex subsurface oxidation regions which were less thick for the second-generation alloys. Elemental compositions of the palladium solid solution matrix in the heat-treated alloys were in good agreement with nominal alloy compositions provided by the manufacturers. Ruthenium-rich particles found in the microstructures of three alloys are consistent with a proposed mechanism for grain refinement.

Key Words: High-palladium dental alloys, dental casting alloys, fixed prosthodontics, scanning electron microscopy, energy-dispersive spectroscopy, dendrite, microstructure, grain refinement, strengthening mechanism, phase diagram.

*Address for Correspondence:
William A. Brantley
Section of Restorative and Prosthetic Dentistry,
College of Dentistry, The Ohio State University
305 West 12th Avenue, Columbus, Ohio 43210-1241
Telephone number: (614) 292-0773
FAX number: (614) 292-9422

Introduction

High-palladium dental alloys [> 70 weight (wt) % Pd] have achieved widespread commercial success over the past decade because of their combination of good mechanical properties and relatively low metal cost, compared to alternative gold-based alloys (Carr and Brantley, 1991). First-generation Pd-Cu-Ga alloys containing ~ 10 wt% Cu and 6-9 wt% Ga date from the patent by Schaffer (1983) for Option, and have much higher values of hardness and yield strength than the more recently marketed second-generation copper-free alloys based upon the Pd-Ga system. While originally developed for metal-ceramic applications, these alloys have been recommended for implant-supported prostheses (Stewart *et al.*, 1992) and removable partial denture frameworks (Asgar, 1988). Compositions of four representative high-palladium alloys are summarized in Table 1. Recent prices for these alloys differ by only ~ 10% from those given by Carr and Brantley (1991).

The high-palladium alloy compositions have been artfully developed by the manufacturers to provide appropriate strength and ductility for clinical applications, while maintaining hardness levels which do not cause undue difficulty for the dental laboratory and clinician in finishing and adjusting the castings (Carr and Brantley, 1991). For metal-ceramic applications which require strong interfacial bonds with dental porcelain (McLean, 1979), these alloys contain the elements Cu, Ga, In, Sn (and perhaps Pd) which form oxides during the initial oxidation ("degassing") heat treatment (van der Zel, 1989). In addition, the alloy compositions have been adjusted by the manufacturers to provide a close match with the ceramic thermal contraction coefficients. This is essential to minimize the subsequent development of residual tensile stresses in the porcelain, when the metal-ceramic restoration is cooled from the porcelain glass transition temperature to room temperature after firing (McLean, 1979).

While the Pd-rich end of the Pd-Ga binary phase diagram provides a useful starting point to consider the physical metallurgy of these dental alloys, the published (Massalski, 1986) phase diagram (Fig. 1) is over thirty years old (Schubert *et al.*, 1959). There are uncertainties about the positions of the liquidus, solidus and sol-

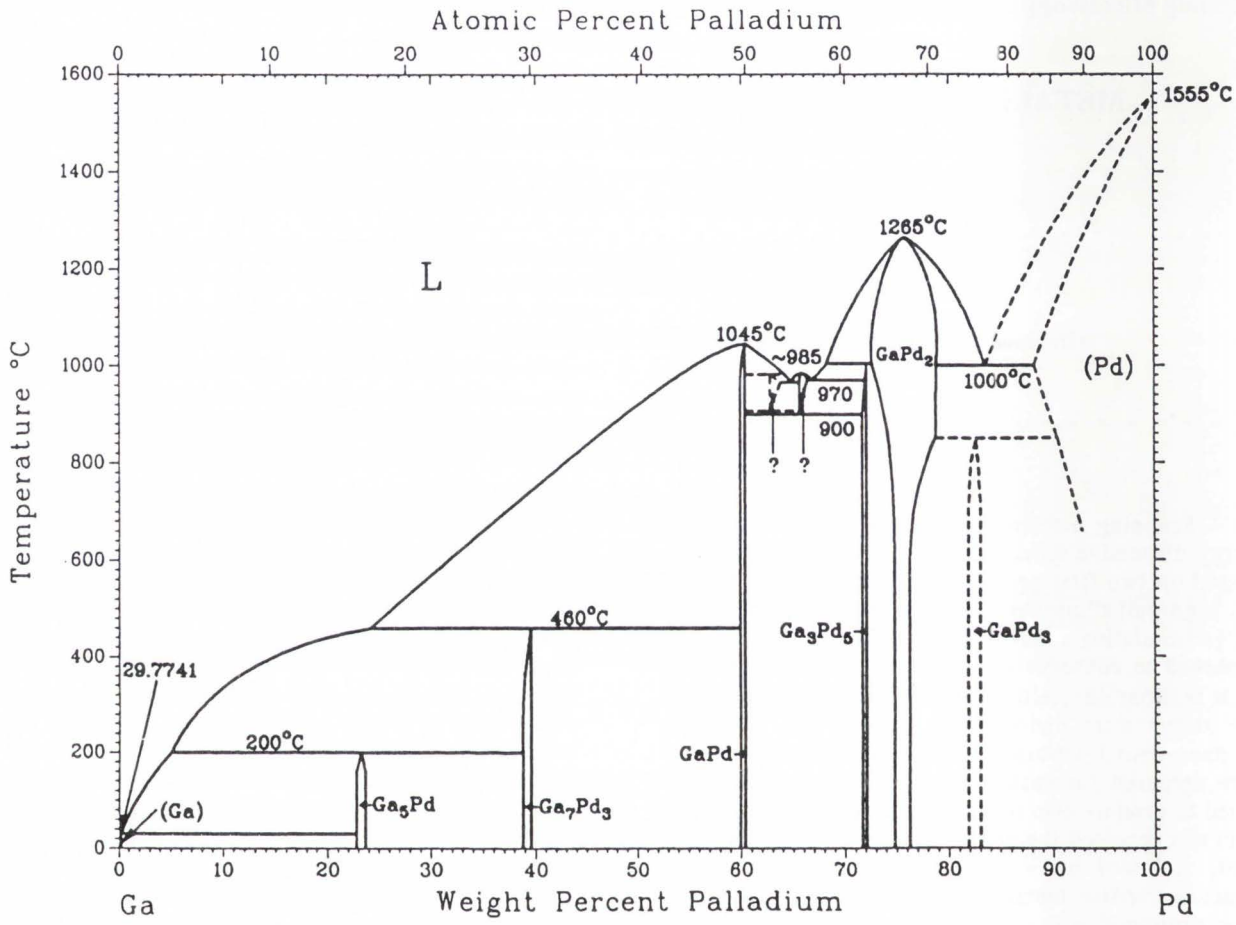

Figure 1. Palladium-gallium phase diagram (Massalski, 1986). Note that the phase designations, such as $GaPd_2$ and $GaPd_3$, are reversed from the style used in this article. Reproduced with permission from ASM International.

Table 1. Nominal† compositions (weight %) of the high-palladium alloys studied (from Carr and Brantley, 1991).

Alloy	Palladium	Copper	Gallium	Gold	Silver	Tin	Indium
Spartan*	79	10	9	2	-	-	-
Protocol*	75	-	6	6	6.5	-	6
Liberty**	76	10	5.5	2	-	~ balance	-
Legacy**	85	-	~ balance	2	1	-	1

†Manufacturer supplied; trace amounts of grain-refining elements were not reported by the manufacturers.
*William Dental, Division of Ivoclar North America, Amherst, NY. **J.F. Jelenko & Company, Armonk, NY.

vus lines, as well as the existence of a peritectoid solid-state transformation involving the formation of Pd_3Ga. Examination of the Pd-Cu phase diagram (Subramanian and Laughlin, 1991) indicates that Cu forms solid solutions with Pd for the Pd/Cu ratios found in the first-generation alloys. A fundamental problem with the use of phase diagrams is that metallurgical structures for dental alloys depart drastically from those expected for equilibrium conditions, because of the rapid solidification rates for typical castings (Phillips, 1991) and the relatively brief period of any post-casting heat treatment such as the porcelain firing cycles. The rapid solidification conditions encountered during the dental casting procedure shift the binary Pd-Ga eutectic reaction to lower weight

percentages of Ga than would occur for very slow cooling under near-equilibrium conditions (Guy and Hren, 1974). Moreover, Cascone (1984) reported that the additions of both copper and indium in the concentration range found for high-Pd dental alloys decrease the solid solubility of Ga in Pd. This effect also shifts the eutectic reaction in Pd-Cu-Ga alloys to lower weight percentages of Ga than for the Pd-Ga binary system.

In recent publications, we have provided extensive information about first-generation and second-generation high-palladium alloys (Carr and Brantley, 1991; Brantley *et al.*, 1992; Carr *et al.*, 1993). Microstructures and measurements of Vickers hardness were presented for the alloys in both the as-cast and heat-treated conditions (simulated porcelain firing cycles). The effects of using a peak investment soak or dwell temperature (mold temperature) during burnout of 1,400° or 1,500°F (760° or 815°C) on the resulting alloy microstructures and hardness were also discussed. The present article describes our continuing research in this area on a more fundamental level than in preceding publications. The objectives of this investigation were to provide new insight into the complex metallurgical structures of as-cast and heat-treated high-palladium alloys and to present novel information about the mechanism for grain refinement in these alloys.

Materials and Methods

The two first-generation (Spartan and Liberty) and two second-generation (Protocol and Legacy) high-palladium alloys listed in Table 1 were selected for study. Standard dental laboratory procedures and manufacturer recommendations were followed for the preparation of cast specimens. Each alloy was melted by multi-orifice gas-oxygen torch in a separate ceramic crucible (Carr and Brantley, 1991). The necessity for fusing the high-palladium alloys in a ceramic crucible has been demonstrated by Hero and Syverud (1985) and by van der Zel and Vrijhoef (1988). The alloys were centrifugally cast in air, using a standard broken arm casting machine (Kerr Division/Sybron Corporation, Romulus, MI).

The specimen design was based upon the coping for a maxillary central incisor restoration and was selected to conserve metal and provide both thin and thick sections, which allowed study of a range of solidification conditions (Carr and Brantley, 1991). Each casting required only ~ 4.5-6 gm (3-4 pennyweights) of alloy, with at least half of the metal used for the sprue system. Wax patterns were invested in a carbon-free, phosphate-bonded investment (Cera-Fina, Whip Mix Corporation, Louisville, KY), and a peak burnout or mold temperature of 1,400°F (760°C) was employed. Three castings were prepared for each of the four alloys. The castings were bench-cooled, devested and air-abraded with 50 μm aluminum oxide particles (APM/Sterngold, Attleboro, MA).

The as-cast specimens were mounted in transparent metallographic resin (Epoxide, LECO Corporation, St. Joseph, MI) and sectioned perpendicular to the sprue base (Carr and Brantley, 1991). This procedure yielded two half-disk specimens which provided mirror-image cross-sections from each original casting. One specimen was carefully removed with a dental handpiece, air-abraded, ultrasonically cleaned in distilled water, and oxidized (Carr *et al.*, 1993). For the two Williams/Ivoclar alloys (Spartan and Protocol), oxidation was carried out in vacuum (i.e., reduced atmospheric pressure in a conventional porcelain furnace) with a five-minute hold at the peak temperature of 1,850°F (1010°C). For the two Jelenko alloys (Liberty and Legacy), oxidation was performed in air with the same peak temperature, but no hold. This step was followed by a simulated full sequence (opaque layer, two body layers and glaze) of porcelain firing cycles (Vita VMK, Vident, Baldwin Park, CA), and the heat-treated specimen was then remounted in resin (Carr *et al.*, 1993).

Following standard metallographic polishing through 0.05 μm alumina slurries, the microstructures of the high-palladium alloy specimens were revealed by etching in *aqua regia* solutions (Mezger *et al.*, 1987). Judicious use of underetching or overetching provided additional information beyond that which we have previously reported about the metallurgical structures of these alloys (Carr and Brantley, 1991; Brantley *et al.*, 1992; Carr *et al.*, 1993).

Specimens were observed in a scanning electron microscope (SEM; JEOL JSM-820, JEOL Ltd., Tokyo, Japan), and scanning electron photomicrographs were obtained in the secondary electron image mode, using a standard Everhart-Thornley detector. Quantitative elemental compositions at selected sites in the alloy microstructures were obtained by X-ray energy-dispersive spectroscopic (EDS) spot and raster analyses. The majority of these analyses were performed with a Tracor-Northern 5500 X-Ray Analyzer (Noran Instruments, Madison, WI), equipped with a Tracor-Northern Micro Z detector and a 5502 upgrade package. Additional EDS analyses were performed with a Link eXL X-ray microanalysis system with a PentaFET detector and ultrathin window (Oxford Instruments Group, High Wycombe, England). Nearly all specimens were coated with a thin carbon layer to prevent electrical charging effects with the metallographic resin disks at high magnifications. Some heat-treated Protocol and Legacy specimens were coated with a thin Au-Pd film to facilitate high-magnification observations of the resin-alloy interfacial regions.

Results

The dendritic as-cast microstructure of the first-generation alloy, Spartan, is depicted in Fig. 2 at greater resolution than in our original article (Carr and Brantley, 1991). Pronounced microsegregation ("coring") has occurred in the palladium solid solution dendrites, which freeze initially when the alloy solidifies. The lighter-contrast peripheries, which were the last

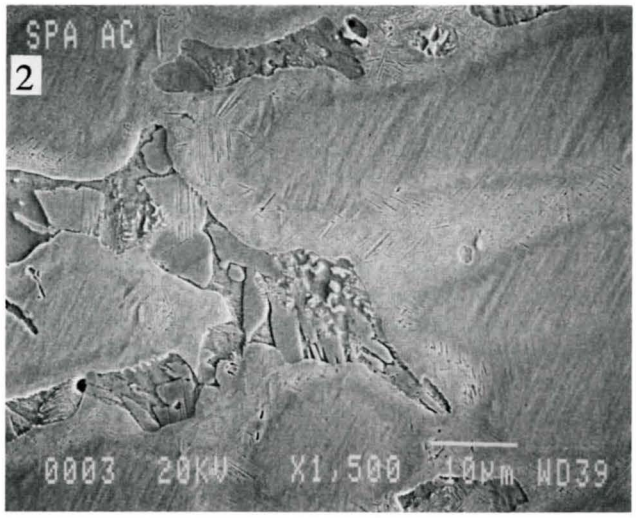

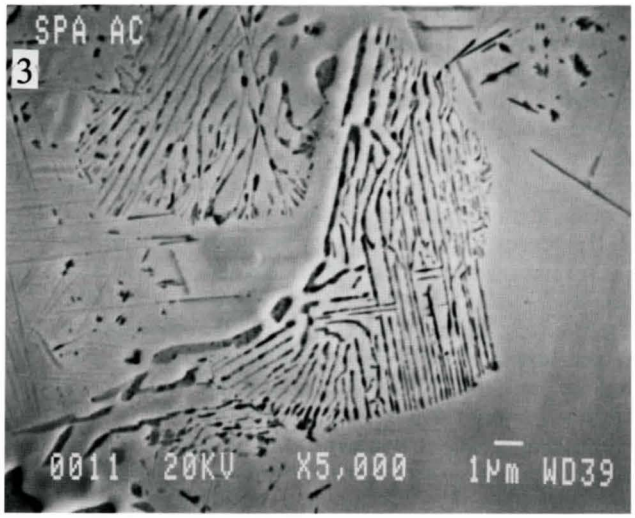

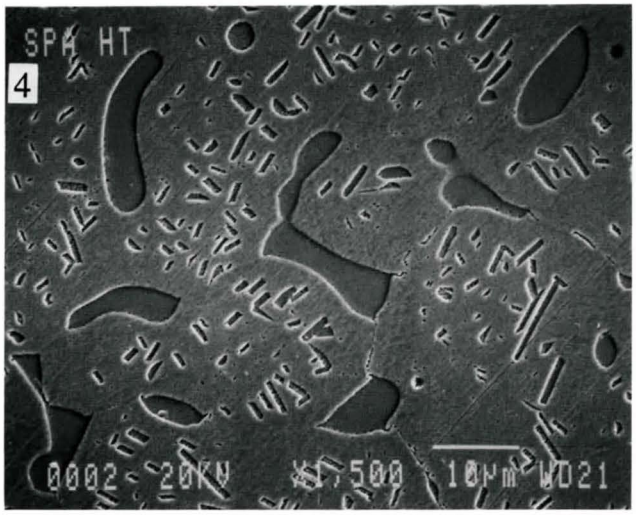

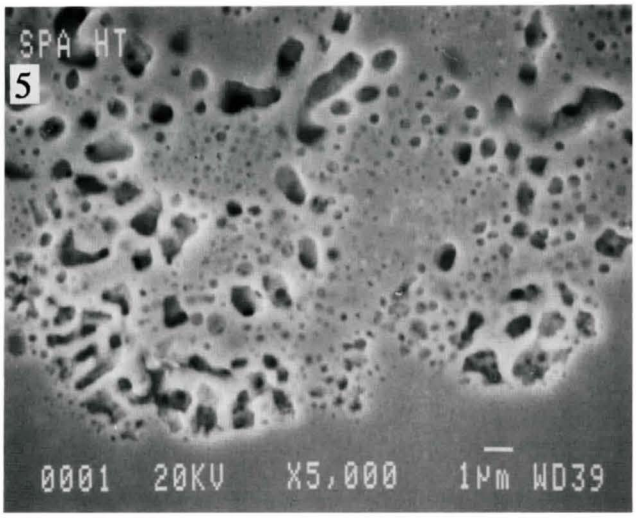

Figures 2-15. Scanning electron micrographs (secondary electron images).

Figure 2. As-cast Spartan. The dendrites exhibit microsegregation and the presence of a needle-like precipitate in the outer portions. The complex nature of the darker contrast interdendritic regions can be clearly seen. Bar = 10 μm.

Figure 3. High-magnification of an area within the interdendritic region for as-cast Spartan. The fine-scale lamellar constituent is based upon the Pd solid solution-Pd_2Ga binary eutectic. Bar = 1 μm.

Figure 4. The bulk coping section for a heat-treated Spartan specimen. The as-cast dendritic structure has disappeared, and at least two secondary phases (dark contrast) coexist with the palladium solid solution phase. The rectangular-shaped phase may have some crystallographic habit. Bar = 10 μm.

Figure 5. The subsurface oxidation region in heat-treated Spartan. EDS analyses suggest that the oxide particles contain Ga_2O_3 and CuO. Bar = 1 μm.

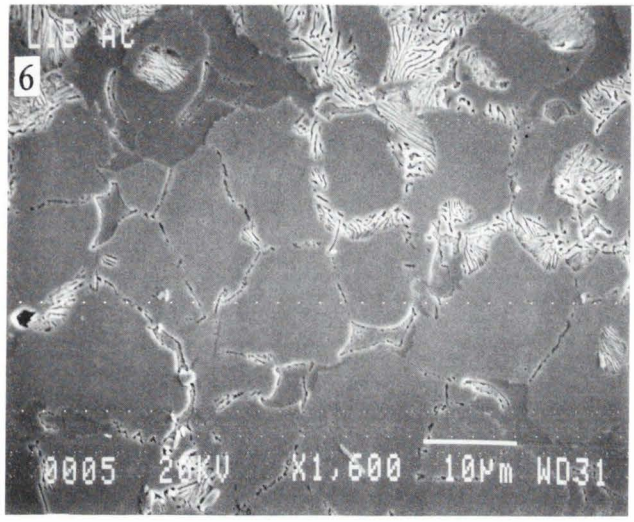

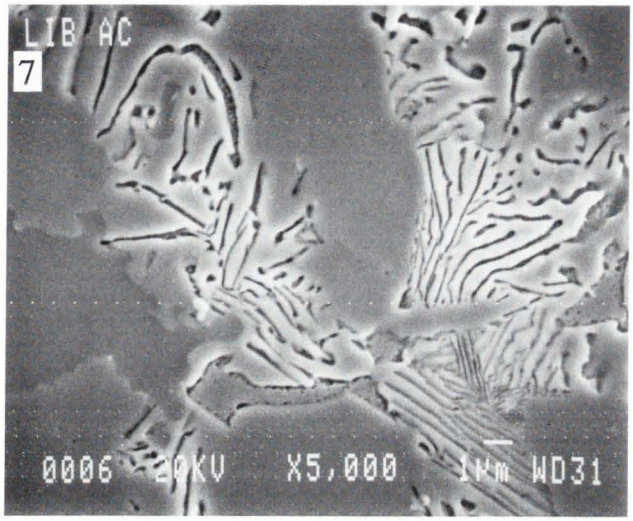

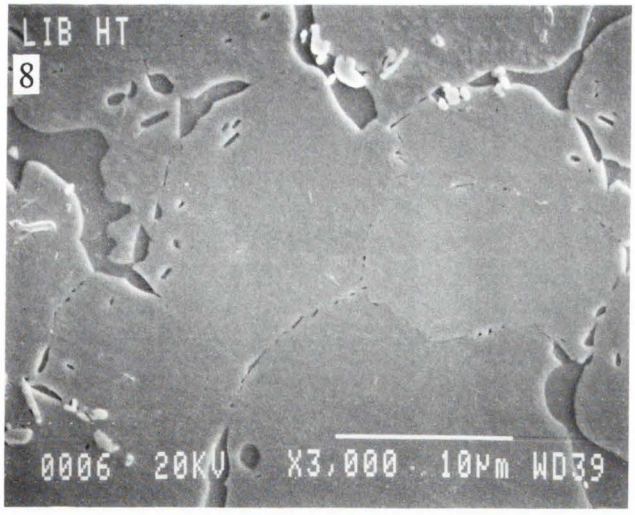

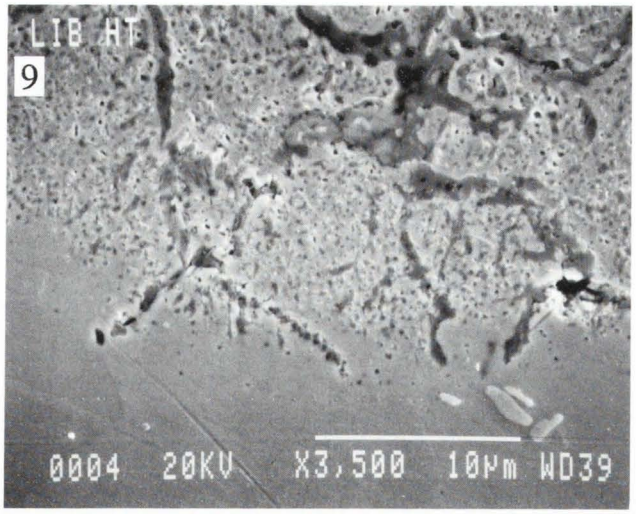

Figure 6. As-cast Liberty, illustrating the transition region between the near-surface and bulk microstructures. In the center of this figure, the Pd solid solution-Pd_2Ga eutectic structure can be seen at some grain boundaries. The eutectic constituent has been removed by the etchant at other sites. Bar = 10 μm.

Figure 7. High-magnification of the eutectic structure near the transition region in Fig. 6 for as-cast Liberty. This micrograph establishes the identity of the unresolved grain boundary precipitate network in our previous publication (Carr and Brantley, 1991). Bar = 1 μm.

Figure 8. The bulk coping section for a heat-treated Liberty specimen. The residual grain boundary eutectic structure has been removed by overetching. The large secondary phase particles which are prominent at the top center and elsewhere in this figure are ruthenium-rich. Bar = 10 μm.

Figure 9. The subsurface oxidation region in heat-treated Liberty (upper portion of figure). EDS analyses indicate that the grain boundary oxide deposits are Ga_2O_3 and suggest that several types of oxide particles may be embedded within the palladium solid solution grains. Bar = 10 μm.

portions of the dendrites to freeze, have the lowest Pd concentration and appear to contain precipitates with a needle-like morphology. Some isolated microscopic porosity was observed within the interdendritic regions, which are the final microstructural constituents of the alloy to undergo solidification. At higher magnification (Fig. 3), the fine-scale interlamellar spacing of < 0.5 μm within some portions of the complex interdendritic regions is apparent. This constituent, which was poorly resolved in our original photomicrographs obtained with the optical microscope and electron microprobe (Carr and Brantley, 1991), is assumed to be a eutectic structure based upon the Pd solid solution-Pd_2Ga binary eutectic (Schubert *et al.*, 1959; Massalski, 1986).

After simulated porcelain firing heat treatment, the dendritic as-cast structure of Spartan was replaced by a completely different bulk microstructure in the coping sections, which is shown in Fig. 4. Morphological differences indicate that at least two secondary phases formed during the heat treatment, and the rectangular phase appears to have some crystallographic habit. An entirely different microstructure was found near the surface of the heat-treated Spartan specimens, where there was a region up to $\sim$ 15 μm thick containing a large number of oxide particles embedded in the palladium solid solution matrix (Fig. 5). EDS analyses indicated increased concentrations of Ga and Cu in the subsurface oxidation region, which suggested that the oxide particles may be composed of Ga_2O_3 and CuO.

The near-surface region of the other as-cast first-generation alloy, Liberty, is dominated by the eutectic structure based upon the Pd solid solution-Pd_2Ga binary eutectic (Carr and Brantley, 1991). Fig. 6 depicts the transition region in as-cast Liberty between the near-surface microstructure and the bulk microstructure, which has been found to have equiaxed grains generally ranging in size from $\sim$ 10-25 μm (Carr and Brantley, 1991). It was not deemed fruitful to attempt to determine an average grain size by standard quantitative metallographic techniques, because of the variation in grain size with thickness of the coping cross-section (Carr *et al.*, 1993). The eutectic structure appears at some grain boundaries in the center of this figure, and there is isolated grain boundary porosity. The delicate nature of the eutectic structure in this region, shown at high magnification in Fig. 7, was poorly resolved in our initial optical microscope and electron microprobe observations of this as-cast alloy (Carr and Brantley, 1991). The fine-scale interlamellar spacing in Fig. 7 and for the near-surface eutectic structure appeared to be approximately the same as that for the interdendritic eutectic constituent in as-cast Spartan (Fig. 3).

After heat treatment, only traces of this eutectic constituent remained at the grain boundaries of Liberty (Carr *et al.*, 1993). Because the microstructure in Fig. 8 was somewhat overetched, the eutectic regions have disappeared due to preferential attack by the etchant. The large secondary phase particles (light contrast from topographic effects) were found to be ruthenium-rich by

Figure 10. An as-cast, somewhat underetched Protocol specimen. Grain boundary voids (from a precipitate network lost during metallographic preparation) and precipitate arrays within grains can be seen. Note the denuded regions near the grain boundaries where these latter precipitates are not found. The grain boundary voids become linked during overetching to yield an apparent equiaxed grain structure. Bar = 10 μm.

Figure 11. The bulk coping section for an overetched, heat-treated Protocol specimen. Precipitates within the grain interiors and at the grain boundaries have been lost during polishing and etching. Bar = 10 μm.

Figure 12. The near-surface region of heat-treated Protocol, showing evidence of Ga_2O_3 grain boundary oxides. Polymerization shrinkage of the metallographic resin has left an interfacial gap at the specimen surface (top of figure). Bar = 1 μm.

Figure 13. As-cast Legacy. This alloy can be etched with much greater facility than as-cast Protocol. The equiaxed grains contain numerous precipitate particles and denuded regions near grain boundaries. Large Ru-rich particles (white appearance), similar to those in Fig. 8, are visible. Bar = 10 μm.

Figure 14. The bulk microstructure for a heat-treated Legacy specimen. The etching has been adjusted to reveal the different configurations found for the secondary phase particles. (The bands within the grains are underetched regions). Large Ru-rich particles, similar to those in Figure. 13, are prominent near the center of the left edge for this figure. Bar = 10 μm.

Figure 15. The near-surface region of heat-treated Legacy. As in Fig. 12, the metallographic resin is at the top of this figure, and there is an interfacial gap between the resin and the specimen surface. From EDS analysis the grain boundary oxide deposits in the center of this figure are again assumed to be Ga_2O_3. Bar = 10 μm.

EDS analysis, which is consistent with the use of Ru as a grain-refining element for high-palladium alloys (Mezger *et al.*, 1987; Vaidyanathan and Prasad, 1987; Walter, 1989). As with Spartan, the subsurface regions of heat-treated Liberty specimens were characterized by a microstructure which was entirely different from that in the bulk coping sections. In Fig. 9 the subsurface oxidation region is $\sim$ 20 μm thick, and there are massive oxide deposits at grain boundaries and large numbers of oxide particles embedded in the palladium solid solution grains. EDS analyses indicated that the grain boundary oxides contained an increased concentration of Ga, and these deposits were interpreted as Ga_2O_3. Increased concentrations of Ga, Cu, In and Sn found within the matrix grains of the subsurface oxidation regions suggest that a variety of oxide particle species may be present (Carr *et al.*, 1993), as previously reported by van der Zel (1989).

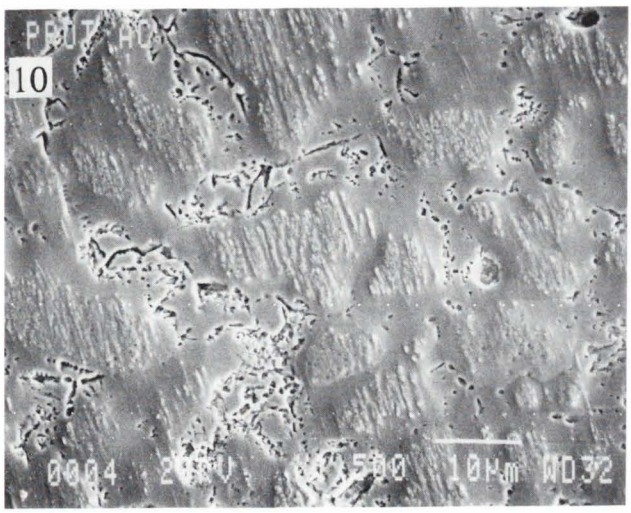
10
0004 20KV X2,500 10µm WD32

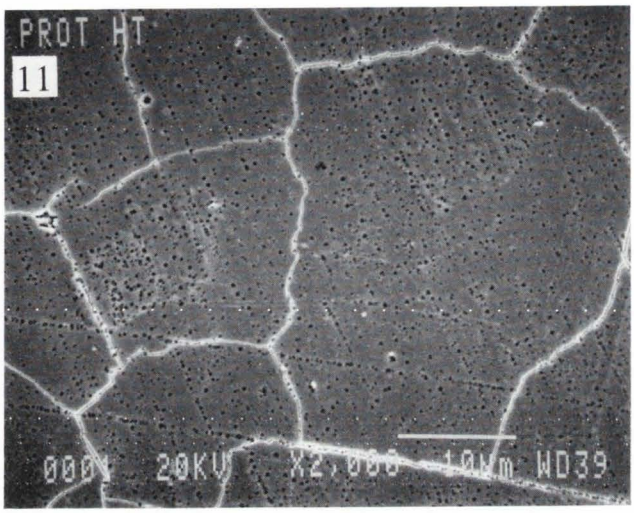
PROT HT
11
20KV X2,000 10µm WD39

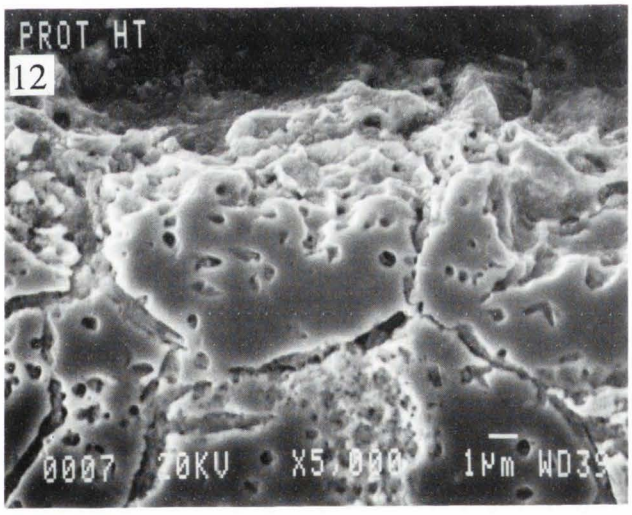
PROT HT
12
0007 20KV X5,000 1µm WD39

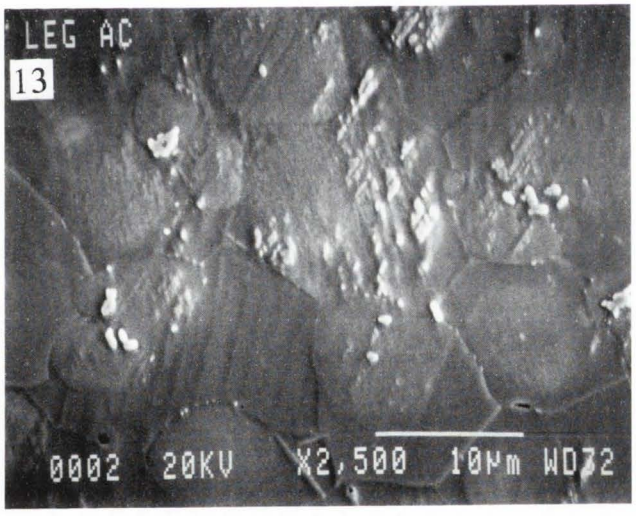
LEG AC
13
0002 20KV X2,500 10µm WD32

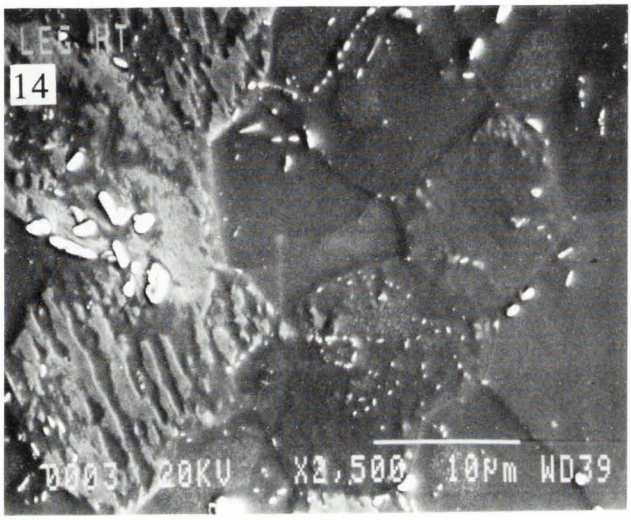
14
0003 20KV X2,500 10µm WD39

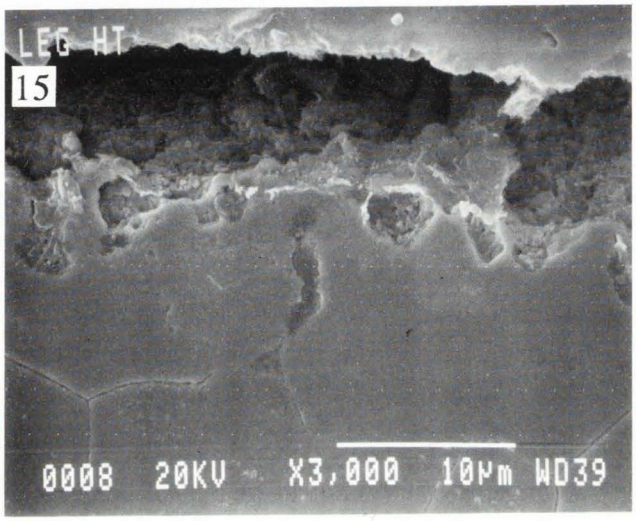
LEG HT
15
0008 20KV X3,000 10µm WD39

Table 2. Vickers hardness measurements* for the high-palladium alloys (adapted from Carr *et al.*, 1993).

Alloy	Condition	
	As-Cast	Heat-Treated
Spartan	403 ± 25	402 ± 14
Protocol	253 ± 5	242 ± 5
Liberty	334 ± 8	285 ± 6
Legacy	294 ± 4	278 ± 4

*Entries are mean value ± standard deviation for measurements with a 1 kg load (n = 10). A burnout temperature of 1,400°F (760°C) was used for fabrication of the cast specimens.

The microstructure of a somewhat underetched, as-cast specimen of the second-generation alloy, Protocol, is displayed in Fig. 10. Well-defined grain boundaries are not evident, and there is an extensive array of secondary phase particles within the grains, along with denuded regions devoid of these precipitates near the grain boundaries (Cai, 1992). There are grain boundary voids where it appears that some unknown phase has been lost during metallographic preparation. With suitable additional etching, these grain boundary artifacts will become linked to yield the equiaxed grain structure previously reported (Carr and Brantley, 1991) for as-cast Protocol when overetched. EDS analysis indicated that large secondary phase particles observed within the grains of this as-cast alloy (not shown in Fig. 10) were Ru-rich, in agreement with our previous electron microprobe results (Carr and Brantley, 1991).

The bulk microstructure of an overetched, heat-treated Protocol specimen is provided in Fig. 11. Extensive observations have established that this alloy also has equiaxed grains ranging in size from ~ 10-25 μm, similar to that for Liberty (Carr and Brantley, 1991; Carr *et al.*, 1993). Numerous voids are present within the grain interiors and along the grain boundaries, where the secondary phase particles in Fig. 10 were lost during polishing and etching. In contrast to the dramatic effects on the as-cast dendritic (Spartan) and eutectic (Liberty) structures for the two first-generation alloys, the simulated porcelain firing heat treatment caused more subtle changes in the bulk microstructure of as-cast Protocol (Carr *et al.*, 1993). However, as in the two other alloys, the near-surface microstructure of heat-treated Protocol was totally different from that in the bulk coping sections. A subsurface oxidation region (Fig. 12) tended to be lost during metallographic preparation and was only occasionally observed at the specimen-resin interface. Moreover, the initially fluid metallographic resin infiltrated the surface oxide and subsequent polymerization shrinkage detached this poorly adhering layer from the alloy, leaving an interfacial gap (Brantley *et al.*, 1992; Carr *et al.*, 1993). The extent of the grain boundary oxide deposits, assumed to be Ga_2O_3 from the elevated Ga concentration obtained by EDS, suggested that the subsurface oxidation region was typically < 10 μm thick, although the thickness in Fig. 12 is ~ 10-15 μm.

The microstructures for Legacy, the other second-generation alloy, generally resembled those for Protocol. Optimal etching of the as-cast microstructure was less difficult for Legacy, and numerous precipitates within grains and denuded regions near grain boundaries can be seen in Fig. 13. Our previous extensive observations have shown that this alloy also has equiaxed grains with sizes from ~ 10-25 μm (Carr and Brantley, 1991), very similar to those for Liberty and Protocol. Faint striations within grains may be associated with compositional fluctuations (Carr and Brantley, 1991) or deformation processes (slip or twinning) (Cai, 1992) during solidification. As with Protocol, as-cast Legacy specimens exhibited minimal porosity (Carr and Brantley, 1991), and the size and shape of these voids suggested an alternative origin from loss of secondary phase particles. The large particles in Fig. 13 were again found to be Ru-rich. While heat treatment appeared to have little effect on the bulk microstructure of Legacy, the amount of etching for Fig. 14 has been adjusted to illustrate the different configurations which were found for the secondary phase particles. These precipitate particles were generally too small for EDS analysis (Carr *et al.*, 1993), although large Ru-rich particles with dimensions similar to those in Fig. 13 were again conspicuous. Fig. 15 shows that the subsurface oxidation region for Legacy contained presumed Ga_2O_3 grain boundary deposits to a depth of ~ 10 μm, and a portion of the adjoining bulk equiaxed grain structure is also visible.

Because of the heterogeneous and fine-scale nature of the microstructural constituents, elemental analyses were not performed on the as-cast alloys and only at selected representative sites in the heat-treated alloys to provide general comparisons to the nominal compositions in Table 1. The approximate concentrations of Pd, Ga and Cu in the bulk matrix grains or regions were in excellent agreement with the alloy compositions reported by the manufacturers (Cai, 1992; Carr *et al.*, 1993). EDS analyses with the Tracor-Northern system indicated relatively large ruthenium concentrations in the bulk matrix grains or regions of all four heat-treated alloys, ranging from ~ 1-4 wt% (Cai, 1992). However, when these analyses were repeated with the Link eXL system, the Ru concentrations were generally below the detection limit of ~ 0.5 wt%. Rhenium, another grain-refining element for high-palladium alloys (Schaffer, 1983; Prasad, 1983), was not detected.

Discussion

The fine-scale microstructures with eutectic constituents for as-cast Spartan and Liberty are striking evidence for the rapid solidification of these alloys under standard dental casting conditions (Carr and Brantley,

1991). For Spartan, the interdendritic regions and outer portions of the palladium solid solution dendrites in Fig. 2 have complex metallurgical structures which are presumably associated with variations in the Pd/Ga ratio during solidification. Our current X-ray diffraction (XRD) studies of as-cast Spartan Plus, which has a composition nearly identical to that of Spartan, may provide information about the structures of these phases (Brantley *et al.*, 1993).

It is tempting to assume that the obstacles to dislocation movement caused by these microstructural constituents provide the dominant hardening and strengthening mechanism for these two first-generation alloys. However, clear evidence that this is not the case has been provided by our recent Vickers hardness measurements (Carr *et al.*, 1993) on the as-cast and heat-treated alloys (Table 2). Although the dendritic structure of as-cast Spartan (Fig. 2) is eliminated by the simulated porcelain firing heat treatment (Fig. 4), there is no corresponding change in hardness and presumably also yield strength (Dieter, 1986). Table 2 also shows that the near-elimination of the eutectic structure in heat-treated Liberty (Fig. 8) only resulted in a decrease in hardness of ~ 15%.

The transmission electron microscopy (TEM) study by Oden and Hero (1986) suggests that the fundamental strengthening mechanism in first-generation high-palladium alloys is complex. These authors presented evidence that the high hardness and strength of an alloy with a composition very similar to that of Spartan arises from local strain fields associated with a complex network of face-centered tetragonal (fct) $Pd_3Ga_xCu_{1-x}$ precipitates < 20 nm thick. These results were consistent with earlier X-ray diffraction experiments by Khabliyev *et al.* (1980) on a non-dental 79Pd-10Cu-9Ga (wt%) alloy also very similar in composition to Spartan. While no XRD evidence was found by Mezger *et al.* (1987) in several commercial high-palladium dental alloys for the fct phases reported by Oden and Hero, the apparent inconsistency is not surprising since this experimental technique has relatively low resolution for secondary phases present in small amounts (Cullity, 1978).

The formation of a submicron $Pd_3Ga_xCu_{1-x}$ precipitate network in the Pd solid solution matrix of first-generation alloys only requires atomic movements over relatively short distances and thus may be plausible. In contrast, a bulk peritectoid reaction similar to that reported in binary alloys (Schubert *et al.*, 1959; Massalski, 1986) for the transformation of Pd_2Ga and the Pd solid solution to Pd_3Ga will be suppressed by rapid solidification conditions. The complex precipitates described by Oden and Hero would likely be stable with heat treatment, thus accounting for the stability of hardness for Spartan in Table 2. Although the as-cast hardness for Liberty is decreased slightly after heat treatment, strengthening mechanisms similar to those for Spartan might be expected since both alloys contain similar amounts of Pd, Cu and Ga (Table 1). It is speculative to link the lower hardness of Liberty with a lower Ga content without detailed knowledge about the strengthening mechanisms.

The nature of the fundamental strengthening mechanisms for the second-generation alloys, Protocol and Legacy, is also conjectural although the greater hardness of Legacy might be related to differences in Ga, Au, Ag, and In contents (Table 1). The much lower hardness of these two alloys, compared to Spartan and Liberty, indicates that some different basic mechanism is involved. The presence of numerous small secondary phase particles within the grains of as-cast Protocol (Fig. 10) and Legacy (Fig. 13) suggests that incoherent precipitates (Dieter, 1986) provide the strengthening mechanism. These precipitates, which form during solidification of the alloys, would not be greatly affected by subsequent heat treatment, accounting for the very small (~ 5%) difference in hardness for the as-cast and heat-treated conditions. While the larger particles within the grains of Protocol and Legacy are Ru-rich, analytical TEM will be required to determine the compositions of the secondary phases.

Although the microstructures of the as-cast second-generation alloys obviously do not represent equilibrium conditions, it is useful to examine appropriate binary phase diagrams (Massalski, 1986) formed by the elemental components and speculate about the compositions of possible phases. Such considerations suggest that Pd-Ga, Pd-Ru and Ga-In phases may form, along with a Pd-In phase in regions where the Pd/In ratio is decreased because of microsegregation. The absence of any eutectic microstructural constituent in the as-cast second-generation alloys, which have Ga concentrations similar to those of the first-generation alloys, confirms the influence of Cu in shifting the position of the binary Pd-Ga eutectic which was reported by Cascone (1984). The actual compositions of phases in the first-generation and second-generation heat-treated alloys may be complex, since under equilibrium conditions each phase must contain some amount of each elemental component, according to the principles of metallurgical thermodynamics (Darken and Gurry, 1952).

German (1982) has reported that the formation of Pd-In, Pd-Ga and Pd-Zn intermetallic compounds appears to provide significant strengthening effects in Au-Pd dental alloys (52-84 wt% Au, 14-37 wt% Pd). He concluded that the very rapid hardening rate for these alloys during heat treatment was due to spinodal decomposition. TEM investigations will be required to determine if submicron precipitates with compositions similar to those reported by German are also found in the high-palladium alloys.

We have recently discussed scanning electron photomicrographs of the heat-treated high-palladium alloys elsewhere (Brantley *et al.*, 1992; Carr *et al.*, 1993) and only the principal metallurgical phenomena will be summarized. The homogenization of the bulk microstructures of the first-generation alloys (Figs. 4 and 8) is accomplished with the aid of high-diffusivity paths in the fine-scale interdendritic (Spartan) and eutectic

(Liberty) constituents. While microstructural effects from heat treatment are much less apparent for the second-generation alloys, there will necessarily be some reduction in residual stresses from solidification and in the as-cast elemental microsegregation (Carr *et al.*, 1993). The latter effect is aided by the relatively short elemental diffusion lengths associated with the fine grain size. The appearance of narrow and well-defined grain boundaries in Protocol after heat treatment (Fig. 11) is a consequence of this reduction in microsegregation.

It was not possible to determine whether the grain sizes of the as-cast high-palladium alloys were significantly altered by heat treatment (Carr *et al.*, 1993). However, from materials science principles, little change in the as-cast grain size would be expected because microsegregation during solidification (Winegard, 1964) should have strong immobilizing effects on grain boundaries (Reed-Hill, 1973) in the as-cast alloys. Moreover, it has been found that the grain size of cast dental gold alloys is not generally affected by subsequent heat treatments (Phillips, 1991).

The complexity of the subsurface oxidation regions arises because each heat-treated alloy contains at least two oxidizable elements (Cu, Ga, In, Sn and perhaps Pd) (van der Zel, 1989). An indirect chemical leaching technique has been employed by van der Zel (1989) to determine compositions of the oxides for several first-generation alloys. While not an objective of this investigation, the composition and thickness of the surface oxide layers on the high-palladium alloys is currently under investigation in our laboratory. Present SEM evidence (Figs. 5, 9, 12 and 15) suggests that the subsurface oxidation region thickness is greater for the first-generation alloys, and may also be greater for an as-cast microstructure with equiaxed grains rather than a dendritic structure (Carr *et al.*, 1993). Our results suggest that the thickness of the subsurface region is not determined by whether the ambient environment for oxidation is air or vacuum (dental porcelain furnace), since Spartan and Protocol were oxidized in vacuum whereas Liberty and Legacy were oxidized in air.

Although the possible role of copper in determining the thickness of the subsurface oxidation regions is conjectural, the greater efficiency of rapid diffusion processes along grain boundaries compared to the interdendritic regions seems plausible. The Ga_2O_3 deposits and grossly widened grain boundaries in Liberty and the two second-generation alloys after heat treatment dramatically demonstrate the major role of grain boundary diffusion processes during alloy oxidation. Suoninen and Hero (1985) have attributed the formation of Ga_2O_3 grain boundary deposits in first-generation alloys to the relatively low free energy of formation for this oxide species. These authors also observed oxide particles with enriched gallium and copper concentrations in the alloy Option, which has essentially the same composition as Spartan (Carr and Brantley, 1991), after bonding to porcelain, in agreement with the present investigation.

The grain-refining element ruthenium appears to have considerable importance for the high-palladium alloys studied in the present investigation, presumably determining whether the as-cast microstructure will be dendritic or have equiaxed grains. While information about the grain-refining techniques employed by manufacturers is proprietary, existing references suggest that the amount of grain-refining element (ruthenium or rhenium) incorporated in the high-palladium alloy compositions does not exceed ~ 0.5 wt% (Schaffer, 1983; Prasad, 1983; Vaidyanathan and Prasad, 1987), which is consistent with our EDS analyses with the Link eXL system. The only high-palladium alloy in the present study where the large ruthenium-rich particles were not prevalent was Spartan. This alloy had a dendritic as-cast microstructure and thus should not contain grain-refining elements. Moreover, because of discrepancies in the other elemental concentrations obtained with the two EDS systems, it was considered that accurate determination of the compositions of the microstructural phases for the four high-palladium alloys would be a difficult task requiring a separate study.

Lastly, from a review of the mechanisms proposed in the materials science literature (Banerji and Reif, 1987), the grain refinement of the high-palladium alloys by ruthenium may be related to the peritectic reaction at the Pd-rich end of the Pd-Ru phase diagram (Massalski, 1986), shown in Fig. 16. Although this proposed model is speculative, particles of a Pd-Ru phase would serve as sites for the subsequent heterogeneous nucleation of the palladium solid solution, which is ordinarily considered the first solid phase to appear in these alloys during solidification. While the ruthenium-rich particles were frequently not observed at the centers of grains, the photomicrographs suggest that these particles could be removed during metallographic procedures and deposited at the grain boundaries. An analogous grain-refining mechanism would be expected for rhenium, since the Pd-Re phase diagram also contains a peritectic reaction at the Pd-rich end (Massalski, 1986). Support for this model will require the use of analytical TEM to determine the compositions of secondary phase particles within the grains and at the grain boundaries of the commercial alloys. Additional studies using model alloy compositions to investigate the mechanism for grain refinement and the compositions of metallurgical phases in high-palladium alloys are planned.

Conclusions

The as-cast microstructures of the four high-palladium alloys studied were consistent with the rapid solidification conditions and the appropriate phase diagrams. Heat treatment simulating oxidation and complete porcelain firing cycles caused homogenization of the two first-generation alloy microstructures along high-diffusivity paths in eutectic or interdendritic constituents. The microstructures of the two second-generation alloys appeared to be minimally affected by heat treatment, other than a decrease in elemental microsegregation. All heat-treated alloys contained subsurface oxidation regions, which were less thick in the second-generation alloys. Bulk matrix compositions determined by EDS for the

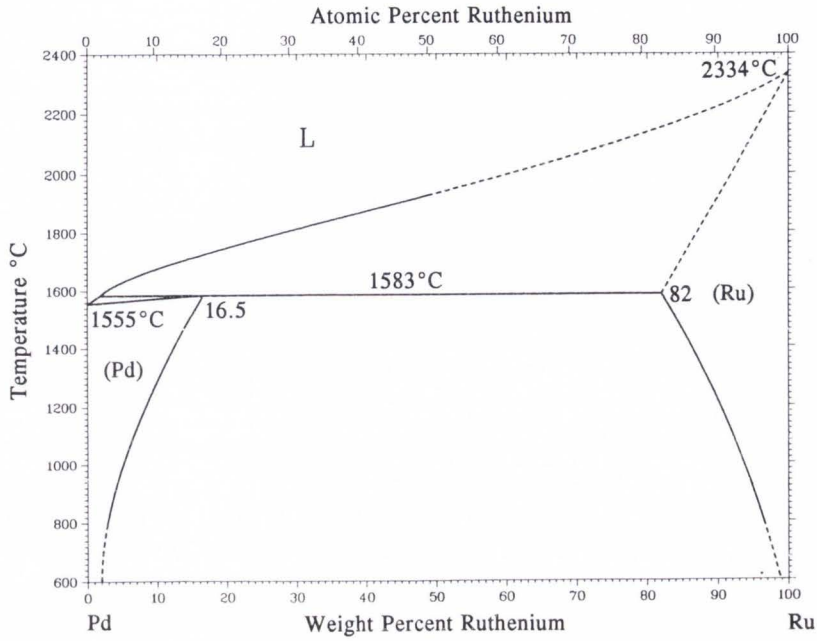

Figure 16. Palladium-ruthenium phase diagram (Massalski, 1986). Reproduced with permission from ASM International.

heat-treated alloys were in good agreement with compositions provided by the manufacturers. A peritectic mechanism consistent with SEM observations has been proposed to account for the grain refinement by ruthenium in these alloys.

Acknowledgment

This investigation was supported by a research grant from the College of Dentistry.

References

Asgar K (1988) Casting metals in dentistry: past-present-future. Adv. Dent. Res. **2**, 33-43.

Banerji A, Reif W (1987) Present situation of grain refinement and its effect on the product quality. Metall. **41**, 393-398.

Brantley WA, Cai Z, Carr AB, Mitchell JC (1992) SEM studies of heat-treated high-palladium alloys. J. Dent. Res. **71**, 626 (IADR Abst. no. 888).

Brantley WA, Cai Z, Carr AB, Papazoglou E, Foreman DW (1993) X-ray diffraction studies of as-cast high-palladium alloys. J. Dent. Res. **72**, 281 (IADR Abst. no. 1420).

Cai Z (1992) A Metallurgical Study of As-Cast and Heat-Treated High-Palladium Dental Alloys. Master of Science Thesis, The Ohio State University.

Carr AB, Brantley WA (1991) New high-palladium casting alloys: Part I. Overview and initial studies. Int. J. Prosthodont. **4**, 265-275.

Carr AB, Cai Z, Brantley WA, Mitchell JC (1993) New high-palladium casting alloys: Part 2. Effects of heat treatment and burnout temperature. Int. J. Prosthodont. (in press).

Cascone PJ (1984) Phase relations of the palladium-base, copper, gallium, indium system. J. Dent. Res. **63**, 233 (IADR Abst. no. 563).

Cullity BD (1978) Elements of X-ray Diffraction (2nd ed). Addison-Wesley, Reading, MA, 407-419.

Darken LS, Gurry RW (1952) Physical Chemistry of Metals. McGraw-Hill, New York, 283-294.

Dieter GE (1986) Mechanical Metallurgy (3rd ed). McGraw-Hill, New York, 212-219, 329-332.

German RM (1982) Precious-metal dental casting alloys. Int. Met. Rev. **27**, 260-288.

Guy AG, Hren JJ (1974) Elements of Physical Metallurgy (3rd ed). Addison-Wesley, Reading, MA, 309-310.

Hero H, Syverud M (1985) Carbon impurities and properties of some palladium alloys for ceramic veneering. Dent. Mater. **1**, 106-110.

Khabliyev SZB, Sakhanskaya IN, Cheremnykh VG, Litvinov VS (1980) Phase transformations in a high-duty alloy of palladium with copper and gallium. Phys. Met. Metall. **47**, 187-189.

Massalski TB (ed) (1986) Binary Alloy Phase Diagrams, Vol. 2. American Society for Metals, 1136, 1153, 1390, 1866, 1868.

McLean JW (1979) The Science and Art of Dental Ceramics. Vol. 1: The Nature of Dental Ceramics and Their Clinical Use. Quintessence, Chicago, 71-72.

Mezger PR, Stols ALH, Vrijhoef MMA, Greener EH (1987) Metallurgical aspects of high-palladium alloys. J. Dent. Res. **67**, 1307-1311.

Oden A, Hero H (1986) The relationship between hardness and structure of Pd-Cu-Ga alloys. J. Dent. Res. **65**, 75-79.

Phillips RW (1991) Skinner's Science of Dental Materials (9th ed). Saunders, Philadelphia, 269-270, 428-429.

Prasad A (1983) Palladium based dental alloys. US Patent 4,412,970.

Reed-Hill RE (1973) Physical Metallurgy Principles (2nd ed). Brooks/Cole Engineering Division,

Monterey, CA, 311-314.

Schaffer SP (1983) Novel palladium alloy and dental restorations utilizing same. US Patent 4,387,072.

Schubert K, Lukas HL, Meissner HG, Bhan S (1959) Zum aufbau der systeme kobalt-gallium, palladium-gallium, palladium-zinn und verwandter legierungen (Concerning the structure of the systems cobalt-gallium, palladium-gallium, palladium-tin, and related alloys). Z. Metallkde. **50**, 534-540.

Suoninen E, Hero H (1985) The structure and oxidation of two palladium ceramic fusing alloys. Biomater. **6**, 133-137.

Stewart RB, Gretz K, Brantley WA (1992) A new high-palladium alloy for implant-supported prostheses. J. Dent. Res. **71**, 158 (AADR Abst. no. 423).

Subramanian PR, Laughlin DE (1991) Cu-Pd (Copper-palladium). J. Phase Equilib. **12**, 231-243.

Vaidyanathan TK, Prasad A (1987) Grain refinement of Pd-based alloys. J. Dent. Res. **66**, 205 (IADR Abst. no. 786).

van der Zel JM (1989). High-Temperature Behavior of Palladium-Based Dental Alloys. Doctoral Thesis, University of Amsterdam.

van der Zel JM, Vrijhoef MMA (1988) Carbon absorption of palladium-enriched ceramic alloys. J. Oral Rehab. **15**, 163-166.

Walter M (1989) Gefügeuntersuchungen verblendeter palladiumlegierungen in der metallkeramischen grenzzone (Structural investigations of veneered palladium alloys in the metal-ceramic interfacial regions). Dtsch. Zahnärztl. Z. **44**, 248-253.

Winegard WC (1964) An Introduction to the Solidification of Metals. Institute of Metals, London, 55-57.

Discussion with Reviewers

H.J. Mueller: Although only small differences existed between the atomic numbers for most of the elements contained in the alloys, was imaging performed by backscattered electrons to attempt to detect differences in composition? Usually, this technique has merit for alloys revealing dendritic formation and coring effects.

Authors: We have performed backscattered electron (BSE) imaging on the as-cast Spartan which has a dendritic microstructure and found that little additional information appeared to be provided beyond that available in secondary electron images. We have found that comparison of the SEI and BSE images were useful for study of the near-surface oxidation regions in the first-generation alloys. These photomicrographs will appear in a forthcoming publication (Carr *et al.*, 1993, in press).

H.J. Mueller: Can the authors comment on the relationship between the subsurface oxidation regions found in the heat-treated high-palladium alloys and the porcelain-metal bonding?

Authors: We have found that the metal-ceramic bonding between these high-palladium alloys and Vita VMK porcelain is significantly better for the first-generation alloys, compared to that for the second-generation alloys (Papazoglou *et al.*, J. Prosthet. Dent., to be published). We are currently employing SEM observations and EDS analyses to investigate the interdiffusion processes and interfacial structure.

H.J. Mueller: Are heat treatments available for these alloys used for implant and removable partial denture applications? It may be desirable to change the yield strength and other mechanical properties, depending upon application.

Authors: This is an important area for future study. However, without knowledge of the fundamental strengthening mechanisms in these alloys, studies to determine appropriate heat treatments will necessarily be empirical.

R.A. Fournelle: The outer regions of the Pd-rich dendrites (not the interdendritic regions) shown in Fig. 2 appear to contain Widmanstätten precipitates. How do the authors account for their formation?

Authors: We concur with this observation. As a consequence of the complex solidification processes for this alloy, these precipitates are expected have a different Pd/Ga ratio than found for the interdendritic constituents. Well-defined (Widmanstätten) orientation relationships between these precipitates and the dendrites are certainly plausible. We are currently investigating the structures of the phases in as-cast Spartan Plus (nearly identical composition to Spartan) by X-ray diffraction and plan to study this matter by transmission electron microscopy.

R.A. Fournelle: The authors suggest that the lamellar structure in the Spartan alloy (Fig. 3) results from eutectic solidification. Although this is feasible from a phase diagram point of view (Fig. 1), morphologically these regions appear to have formed by boundary migration, i.e., by discontinuous precipitation. Indeed, in the Discussion of the microstructure of the Liberty alloy (Figs. 6 and 7), the authors seem uncertain as to whether the lamellar structure should be considered eutectic or discontinuous precipitation. Can the authors comment in more detail about these structures?

Authors: From our present experiments we are unable to comment on the detailed mechanisms for the formation of the lamellar structures in as-cast Spartan and Liberty. While we have adopted the eutectic constituent designation for these two alloys, it may indeed be possible that these structures have formed by means of discontinuous precipitation through boundary migration processes. This is an interesting area for further study in the physical metallurgy of these complex alloys.

R.A. Fournelle: In Fig. 10 there appear to be precipitate-free zones near the grain boundaries. Could the authors comment on their origin?

Authors: We have noticed these zones (Cai, Master of Science Thesis, 1992, Ohio State Univ.), but are currently unable to provide comments about their origin other than noting a linkage with the grain boundary precipitate network which was removed by etching.